

Cite this: *Soft Matter*, 2011, **7**, 5585

www.rsc.org/softmatter

PAPER

Hyperdiffusive dynamics in conjugated polymer blends and fullerene absorbing solutions

Olga D. Parashchuk,^{ab} Tatyana V. Laptinskaya,^a Maria S. Ananieva^a and Dmitry Yu. Parashchuk^{*ab}

Received 25th March 2011, Accepted 1st April 2011

DOI: 10.1039/c1sm05519d

We have observed the hyperdiffusive dynamics of light scatterers accompanied by their ballistic motion by a dynamic light scattering (DLS) technique in blends of semiconducting polymer (poly[2-methoxy-5-(2-ethylhexyloxy)-1,4-phenylenevinylene], MEH-PPV) with a low-molecular-weight organic acceptor 2,4,7-trinitrofluorenone, TNF) and in fullerene C₆₀ solution. The DLS autocorrelation function has been found to follow the Kohlrausch-Williams-Watt function with the exponent β in the range of 0.5–2, depending on the laser power, scattering vector, optical absorption and type of sample. We show that the hyperdiffusive dynamics ($\beta > 1$) results from laser-induced convection caused by optical absorption at the DLS probing wavelength. The convection appears in the DLS data as a ballistic motion with velocities in the range of 5–60 $\mu\text{m s}^{-1}$ depending on the laser power, type of sample and their absorption. The convection is driven by the local temperature difference, $\Delta T \sim 0.1\text{--}0.2$ K, as evaluated from thermal lens effect measurements. We demonstrate that by decreasing the absorbed laser power, laser-induced hyperdiffusion can be avoided in both the polymer and fullerene samples so that the inherent thermal molecular motion can be probed. Specifically, in the polymer solutions, we have found a slow relaxation mode with the characteristic spatial spectrum of the inverse relaxation time $T_s \propto q^4$. This mode has been assigned to the coupled motion of entangled conjugated polymer chains.

I. Introduction

Dynamic light scattering (DLS) is widely used for the investigation of molecular dynamics in the liquid phase. The intensity autocorrelation function (ACF) of light scattered from the concentration fluctuations provides information about a broad range of different types of molecular motions; from the diffusion of individual molecules to the large-scale coupled motion of entangled polymer chains. The light scattered from particles under thermal Brownian motion in dilute solution is described by an exponential ACF. More complicated motions, *e.g.*, interconnected fluctuations of entangled polymer chains in semidilute solutions, could be described by a stretched exponent.^{1–10} In many suspensions, gels and semidilute polymer solutions, the intensity ACF, $G_2(t)$, exhibits a two-step decay described by the Kohlrausch-Williams-Watt (KWW) function:^{6,11–15}

$$G_2 - 1 = (A \times \exp - (t/\tau_f) + (1 - A) \times \exp - (t/\tau_s)^\beta)^2, \quad (1)$$

where $\tau_{f,s}$ are the characteristic times of fast and slow relaxations, respectively, A is the amplitude of the fast mode, β is the Kohlrausch exponent. The common diffusion motion in dilute

solution corresponds to the mono-exponential decay that is described in the KWW approach. The type of relaxation, *e.g.*, diffusion, reptation, *etc.*, can be determined from the experimental dependence of the characteristic inverse relaxation time, $\Gamma = 1/\tau$, on the scattering vector, $q = (4\pi n/\lambda)\sin(\theta/2)$,^{1,14,15} where n is the refractive index, λ is the excitation wavelength and θ is the scattering angle. This dependence can be fitted by a power function $\Gamma \sim q^\alpha$. For example, $\alpha = 2$ corresponds to common diffusion,¹¹ $\alpha = 1$ is interpreted as ballistic motion.¹⁶

In semidilute polymer solutions, the fast decay parameter, $\Gamma_f = 1/\tau_f$, is usually due to the cooperative diffusive motion in blobs which are roughly defined as the polymer segments between two neighboring cross-linking points.¹⁷ The diffusion in blobs is characterized by the q^2 -dependence ($\alpha = 2$) of Γ_f . The slow relaxation time, τ_s , in various semidilute polymer solutions was previously assigned to different physical reasons:⁶ the q -independent ($\alpha = 0$) viscoelastic relaxation of a polymer network,^{18,19} the q^2 -dependent ($\alpha = 2$) translational diffusion of large aggregates,^{3,5,18,19} the reptation of the entire polymer chain inside a “tube” made of its surrounding chains.^{12,18,19} The Rouse relaxation, which is the stretching and compression of some parts of the macromolecules along the tube axis,⁵ and the reptation relaxation of the entangled polymer chains were theoretically predicted earlier¹⁴ and characterized by different values of α (from 0 to 4) in the different scattering vector ranges.⁵

^aFaculty of Physics, Lomonosov Moscow State University, Moscow, 119991, Russia. E-mail: paras@physics.msu.ru

^bInternational Laser Center, Lomonosov Moscow State University, Moscow, 119991, Russia

In all the mentioned cases, the slow dynamics is slower than the exponential relaxation, which corresponds to $\beta < 1$ in the KWW function and is referred to a subdiffusive dynamics. However, in some soft matter systems, the slow relaxation is described by an unusual compressed exponential function where $\beta > 1$, which is a signature of hyperdiffusive dynamics. The hyperdiffusive dynamics were observed using DLS or X-ray photon correlation spectroscopy (XPCS) in a wide range of systems: colloidal fractal gels,²⁰ concentrated emulsions,²⁰ lamellar gels,^{20,21} micellar polycrystals,²⁰ highly viscous polymer melts,²¹ bicontinuous phases of block copolymers,^{22,23} nanocomposites^{24,25} and nanoparticles suspended in the glass-forming liquid.²⁶ The hyperdiffusive dynamics are characterized by a q -dependent ($\alpha = 1$) slow decay parameter, $\Gamma_s = 1/\tau_s$,^{16,20,27,28} that indicates ballistic motion with a characteristic velocity V .²⁶ The typical values of β were usually found to be in the range of 1.3–2.^{16,22–27,29} The origin of hyperdiffusive dynamics is under discussion (*e.g.*, Ref. 30). On the one hand, two explanations related to the intrinsic processes in the sample have been suggested: the continuous time random walk model^{28,31,32} and the model of stress-field relaxation.^{20,33} On the other hand, hyperdiffusive dynamics can be associated with radiation damage of the sample during the XPCS experiment.³⁰

In this paper, we report on the observation of hyperdiffusive dynamics in solutions of π -conjugated molecules and address its origin. We show that hyperdiffusion can result from laser-induced convection in solutions absorbing at the DLS wavelength. By using two different types of samples, namely conjugated polymer donor–acceptor blends and fullerene C₆₀, we demonstrate that the absorption of the DLS laser beam can induce convection, resulting in the hyperdiffusive dynamics of light scatterers, along with their ballistic motion. We analyze how the laser-induced convection can be avoided in DLS in order to probe the inherent thermal molecular motions. Specifically, we have found a q^4 -dependent slow relaxation mode in polymer solutions, both absorbing and non-absorbing at the DLS wavelength.

As was shown in earlier DLS studies, if the sample absorbs at the DLS probing wavelength, the absorption may lead to the experimental errors and the underestimation of the correlation length³⁴ as a result of laser-induced convection. The DLS studies of absorbing systems were previously carried out on colloidal particles containing tiny gold clusters,³⁵ a solution of polyaniline and a complex of cytochrome *c* and cytochrome *c* peroxidase in a phosphate buffer,³⁶ and a blue-colored polystyrene latex.³⁴ If the laser irradiation causes heating and convection, the corresponding exponential ACFs may show oscillations that can be described by the modulated exponential function.³⁵ The values of the convective flux velocities obtained were 1 mm s⁻¹, Ref. 35, and 0.4 mm s⁻¹, Ref. 36, for a laser power of ~ 250 mW and absorbance of ~ 1 cm⁻¹. As shown below, in our samples the oscillations in the ACF are not observed. In our experiments, the convection appears as hyperdiffusive dynamics accompanied by ballistic motion, and we determine the convective velocities from the spatial spectra of the corresponding relaxation times. To substantiate that the hyperdiffusion is laser induced, we have performed thermal lens measurements and estimated the thermal gradient as the convection driving force.

We have investigated two absorbing solutions: fullerene C₆₀ solution and a donor–acceptor blend of a semiconducting polymer poly[2-methoxy-5-(2-ethylhexyloxy)-1,4-phenylenevinylene] (MEH-PPV) with a low-molecular-weight organic acceptor 2,4,7-trinitrofluorenone (TNF). The blend absorption at the DLS probing wavelength is caused by the ground-state charge-transfer complex formed between the donor (MEH-PPV) and acceptor (TNF).^{37–39} We show that the polymer and fullerene samples demonstrate very similar hyperdiffusive dynamics, which is mainly controlled by the absorbed laser power.

The paper is organized as follows. In Sec. II, the DLS data is presented. In Sec. III, we explain the observed hyperdiffusive dynamics in terms of convection. Then, to identify the convection driving force, we analyze the results of the thermal lens measurements. Finally, we discuss the inherent thermal molecular dynamics observed at a low laser power. In Sec. IV, the experimental details are given.

II. Experimental results

A. Polymer samples

To highlight the effect of absorption at the DLS wavelength (633 nm) on the DLS data, we compare below the data for MEH-PPV, which is practically non-absorbing at 633 nm, and MEH-PPV:TNF blends, which are moderately absorbing at 633 nm.

Fig. 1 presents the DLS data for the pristine polymer solution, MEH-PPV, and for the MEH-PPV:TNF = 1 : 0.15 blend in chlorobenzene. Fig. 1(a) plots the ACFs and the corresponding fits by the KWW function (solid lines) [eqn (1)], which fits perfectly with the experimental data. The pristine MEH-PPV exhibits the slow dynamics characteristics of a semidilute solution^{1,3,5–7,9,13,18–19,40–43} where the slow relaxation of entangled polymer chains can be described by an extended ACF with a stretched exponent ($\beta < 1$). Fig. 1(b) shows β as a function of the scattering vector, q , (*i.e.*, the spatial spectrum) for the pristine polymer. As q increases, β falls monotonically from 0.95 to ~ 0.5 and becomes independent of q at $q \geq 0.02$ nm⁻¹ ($\theta \geq 90^\circ$). Such a spatial spectrum is evidence of sub-diffusion. The value $\beta \sim 0.5$ was theoretically predicted for the macromolecular dynamics in a semidilute solution.¹⁴ The inset in Fig. 1(c) shows the q^2 -dependence of the fast relaxation, $\Gamma_f(q) \propto Dq^2$, with a diffusion coefficient of $D = (1.7 \pm 0.4) \times 10^{-7}$ cm² s⁻¹. We assign the fast dynamics in pristine MEH-PPV to the cooperative diffusive fluctuations of polymer chains in a semidilute solution^{1,3,5,6,44} that are usually termed as blob fluctuations. As Fig. 1(c) illustrates, the slow relaxation, Γ_s , is q^4 -dependent, *i.e.*, $\Gamma_s(q) \propto Aq^4$. The q^4 -dependence was predicted for the Rouse mode⁵ in a much higher range ($q = 0.1–0.3$ nm⁻¹) than we have used ($q = 0.005–0.03$ nm⁻¹). The q^4 -dependence was not observed earlier, and it was not predicted in our range of q . In non-conjugated polymers, other various motions have been observed and predicted in this range of q .^{5,6} Therefore, one can suggest that the q^4 -dependence of the slow mode appears in the semidilute solution of conjugated polymer and characterizes the slow dynamics of entangled π -conjugated chains. Importantly, the DLS data for the pristine polymer does not depend on the laser power, P , whereas it does in the polymer-acceptor blend (Fig. 1(d)). First,

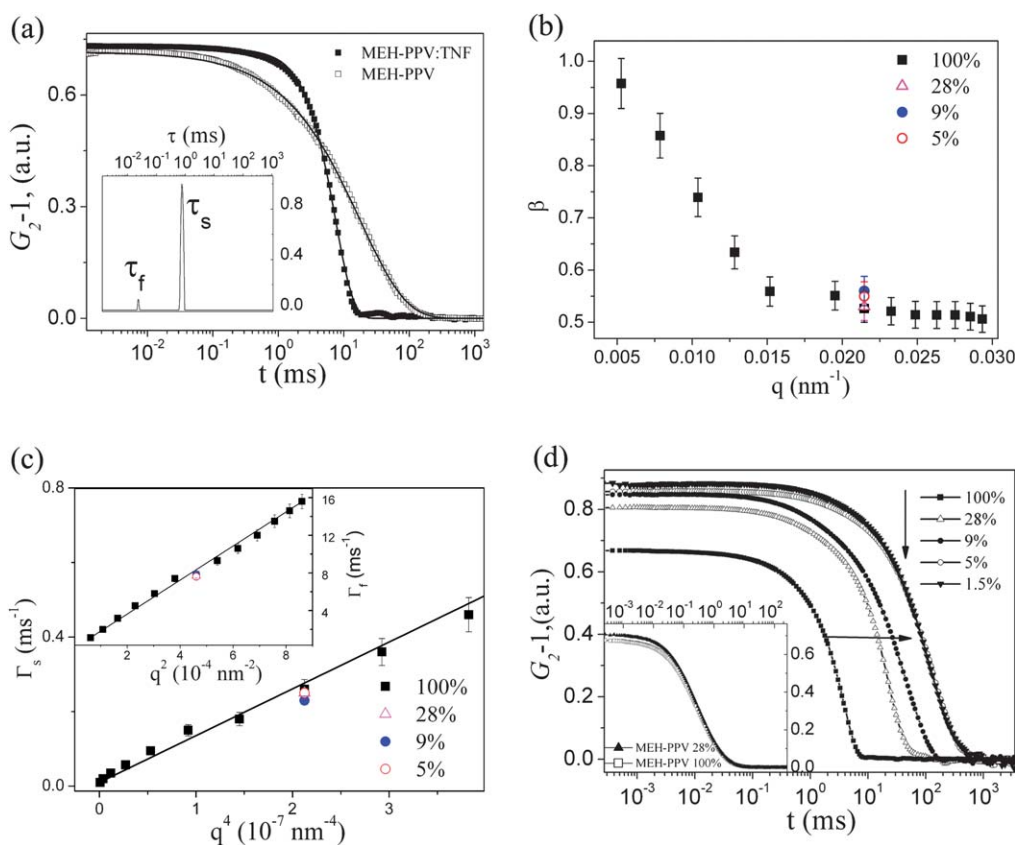


Fig. 1 DLS data for pristine MEH-PPV and MEH-PPV:TNF = 1 : 0.15 blend in chlorobenzene. (a) ACFs for the pristine MEH-PPV (open squares) and for the blend (full squares) measured at the scattering vector $q = 0.005 \text{ nm}^{-1}$ and 100% laser power. The solid lines are the KWW fits with $\beta = 0.96$ for the pristine MEH-PPV and $\beta = 2$ for the blend. The inset shows the relaxation time distribution calculated with the use of the CONTIN software for the blend. (b) Spatial spectrum of β for the slow mode in the pristine MEH-PPV. The colored points show β for different laser powers at $q = 0.022 \text{ nm}^{-1}$. (c) Slow relaxation parameter, Γ_s , as a function of q , the solid line is a fit by $\Gamma_s = Aq^4$ where $A \sim 10^{-19} \text{ cm}^4 \text{ s}^{-1}$. The inset shows the fast relaxation parameter, Γ_f , as a function of q , the solid line is a fit by $\Gamma_f = Dq^2$ where $D = (1.8 \pm 0.1) \times 10^{-7} \text{ cm}^2 \text{ s}^{-1}$. The colored points show Γ_s and Γ_f for different laser powers. (d) ACFs for the blend measured at different laser powers at $q = 0.0075 \text{ nm}^{-1}$. The inset shows the ACFs for the pristine MEH-PPV measured for different laser powers at $q = 0.022 \text{ nm}^{-1}$. The solid lines are the KWW fits.

we discuss the data for $P = 20 \text{ mW}$ (we will refer to this power as to 100% one), the data for $P < 100\%$ is given at the end of this section.

The ACF is dramatically changed upon the addition of the acceptor (Fig. 1(a)): it falls faster than the exponential function and can be well approximated by a compressed exponent ($\beta > 1$). The CONTIN software applied to the ACF gives two relaxation times: the fast ($1/\Gamma_f$) and the slow ($1/\Gamma_s$) ones. The relaxation parameters of these modes (Γ_f , Γ_s) obtained from both the CONTIN and KWW fits are the same.

Fig. 2 presents the spatial spectra of $\Gamma_{f,s}(q)$ and the exponent parameter for the slow mode, $\beta(q)$, in the MEH-PPV:TNF blends. Fig. 2(a) and (b) show the q^2 -dependencies of Γ_f in MEH-PPV:TNF = 1 : 0.15 and MEH-PPV:TNF = 1 : 0.2 blends, respectively. In both, the fitting by $\Gamma_f(q) \propto Dq^2$ results in the diffusion coefficients $D = (1.9 \pm 0.1)$ and $(2.0 \pm 0.2) \times 10^{-7} \text{ cm}^2 \text{ s}^{-1}$, respectively. These diffusivities coincide with each other and also with that of the pristine polymer; hence, they could be assigned to the one process, specifically, diffusion in blobs. Therefore, one can conclude that the fast relaxation has not been changed upon TNF addition.

Fig. 2 (c) and (d) show the q -dependencies of the slow relaxation parameter, Γ_s , for the MEH-PPV:TNF = 1 : 0.15 and MEH-PPV:TNF = 1 : 0.2 blends, respectively. The linear dependence $\Gamma_s = Vq$ observed for the blends at $q < 0.023 \text{ nm}^{-1}$ is a fingerprint of ballistic motion with characteristic velocities of $V = 19$ and $29 \text{ } \mu\text{m s}^{-1}$ for MEH-PPV:TNF = 1 : 0.15 and MEH-PPV:TNF = 1 : 0.2, respectively. One can see that the higher the acceptor content, the higher the velocity. We relate this to the increasing absorption of the blend with the increasing acceptor content (see Table 1). The spatial spectrum of Γ_s up-diverges from the straight line at $q > 0.023 \text{ nm}^{-1}$ (Fig. 2 (c)). One can conclude that the slow relaxation has a different origin in the pristine ($\Gamma_s \sim q^4$) and blended ($\Gamma_s \sim q$) solutions. As was discussed above, in the pristine polymer, the slow relaxation can be assigned to the large-scale interconnected motions of the entangled π -conjugated chains, whereas, in the blend, the slow relaxation appears to be a ballistic motion. The ballistic motion differs from diffusion,^{16,20,21} in that the scatterer displacement grows linearly with time, t , whereas it grows as $t^{1/2}$ for diffusion. The ballistic motion was observed in a number of soft matter systems.^{16,21–26} In all the studied systems, the linear dependence

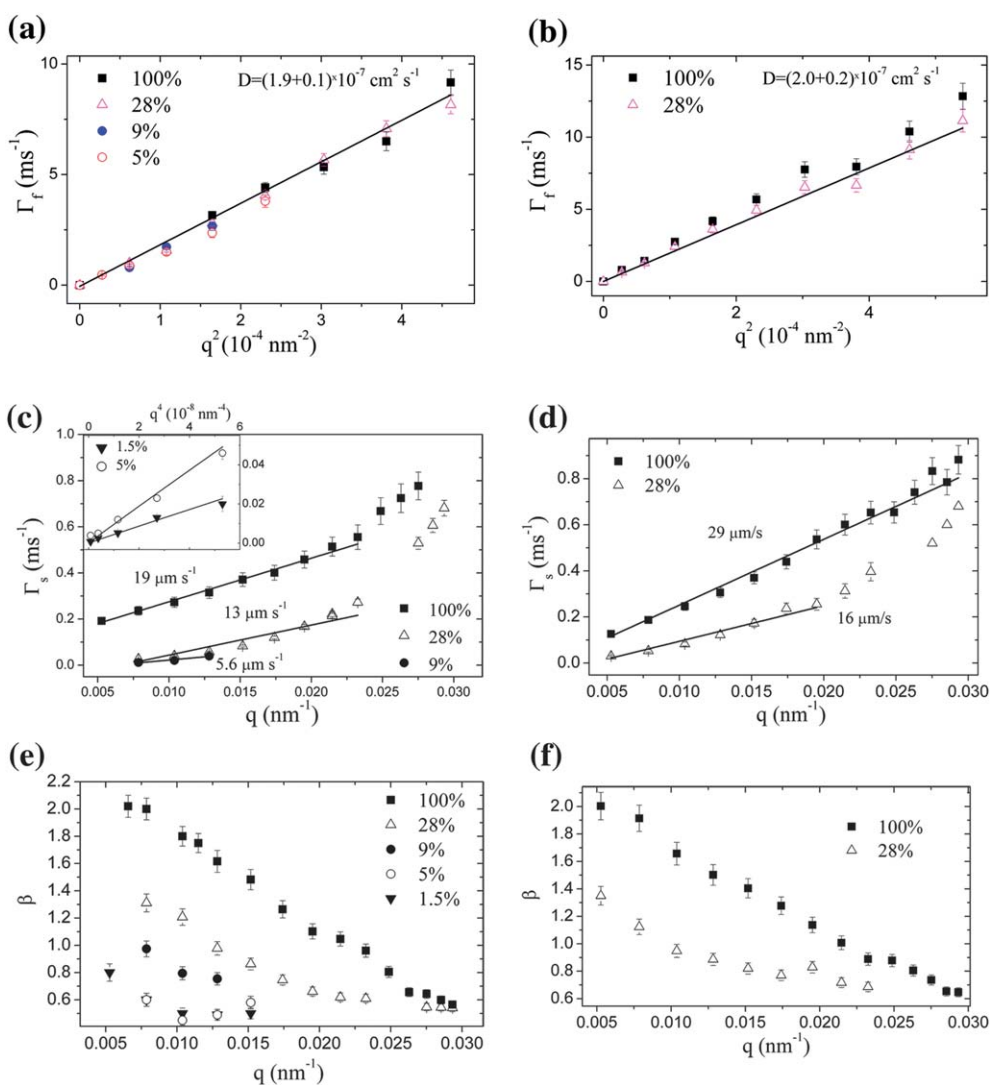


Fig. 2 Spatial spectra of the relaxation parameters (Γ_f , Γ_s) and the exponent of the slow mode, β , in the MEH-PPV:TNF blends in chlorobenzene for different laser powers. Γ_f vs. the scattering vector, q , for MEH-PPV:TNF = 1 : 0.15 (a) and MEH-PPV:TNF = 1 : 0.2 (b). The solid lines represent fits by $\Gamma_f = Dq^2$, with D indicated in the graphs. Γ_s vs. q for MEH-PPV:TNF = 1 : 0.15 (c) and for MEH-PPV:TNF = 1 : 0.2 (d). The solid lines are fits by $\Gamma_s = Vq$ with V indicated in the graphs. The inset shows the data for the laser power at 5% and 1.5% with their fits by $\Gamma_s = Aq^4$, $A = 8 \times 10^{-20}$ and $4 \times 10^{-20} \text{ cm}^4 \text{ s}^{-1}$, respectively. The slow exponent, β , vs. q for MEH-PPV:TNF = 1 : 0.15 (e) and for MEH-PPV:TNF = 1 : 0.2 (f).

$\Gamma(q)$ was accompanied by a compressed-exponential ACF with β in the range of 1.3–2.^{16,21,26,27,29} In the blends, we also have observed that the linear dependence $\Gamma_s(q)$ was accompanied by a compressed-exponential ACF. Fig. 2 (e) and (f) present β for the slow mode as a function of q for MEH-PPV:TNF = 1 : 0.15

and MEH-PPV:TNF = 1 : 0.2. Surprisingly, at the smallest scattering vector ($q = 0.005 \text{ nm}^{-1}$, scattering angle $\theta = 20^\circ$), the slow relaxation is characterized by a Gaussian ACF, *i.e.*, $\beta = 2$. As q is increased, β falls monotonically from two to values below unity (~ 0.6). The value of β becomes smaller than unity at

Table 1 Absorption coefficients α at a wavelength of 633 nm, convective (ballistic) velocities V , the ratio $(\partial n/\partial T)/\kappa$, the local change in refractive index Δn and in temperature ΔT for the studied samples

	MEH-PPV	MEH-PPV:TNF = 1 : 0.15	MEH-PPV:TNF = 1 : 0.2	C_{60}
$\alpha \text{ (cm}^{-1}\text{)}$	0.01	0.3	0.4	0.5
$V \text{ at } P = 100\% \text{ (}\mu\text{m s}^{-1}\text{)}$	n/a	19	29	65
$\frac{\partial n}{\partial T} \frac{1}{\kappa} \times 10^{-1} \text{ (cmW}^{-1}\text{)}$	n/a	1.1 ± 0.1	n/a	1.7 ± 0.1
$\Delta n \times 10^{-5}$	n/a	1.3 ± 0.2	n/a	3.5 ± 0.4
$\Delta T \text{ (K)}$	n/a	0.10 ± 0.01	n/a	0.20 ± 0.02

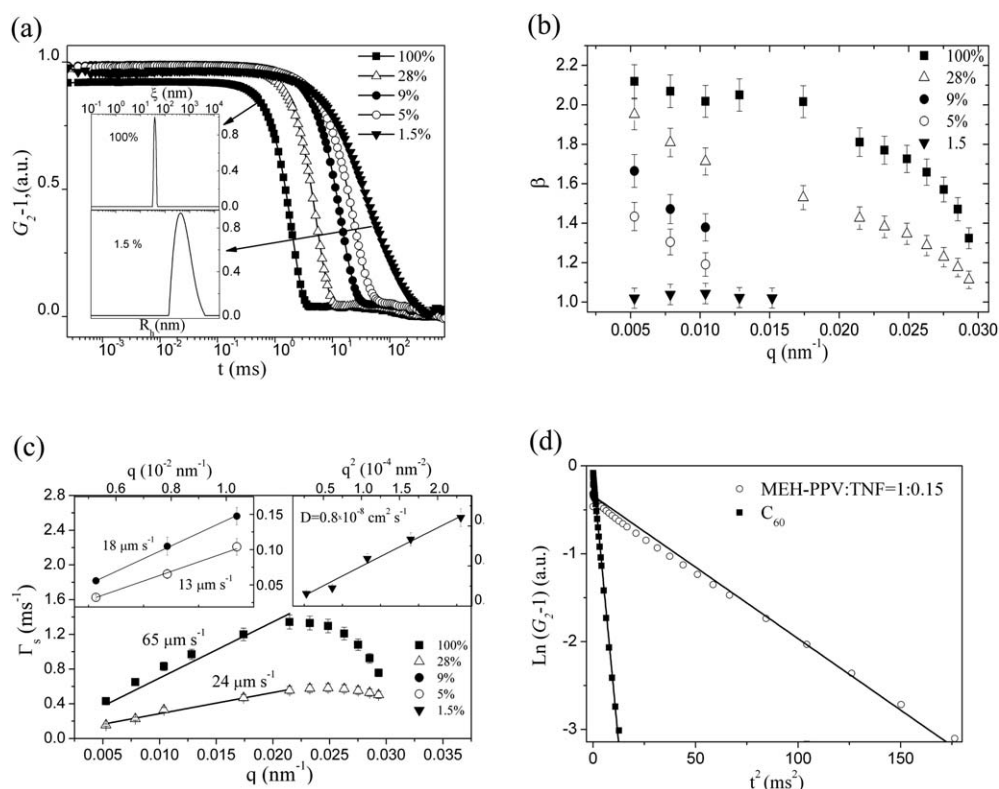


Fig. 3 DLS data for C_{60} . (a) ACFs measured at $q = 0.005 \text{ nm}^{-1}$ for different laser powers. The solid lines are the KWW fits. The insets show the correlation length ξ and hydrodynamic radius R_h distributions calculated by the CONTIN software with 100% and 1.5% powers, respectively. (b) The exponent, β , vs. the scattering vector q . (c) Relaxation parameter, Γ_s , vs. q with the laser powers 100% and 28%. The solid lines are $\Gamma_s = Vq$ dependencies with V indicated in the graph. The left inset shows the data for laser powers 9% and 5% with their fits by $\Gamma_s = Vq$. V is indicated in the graph. The right inset shows q^2 -dependencies of Γ_s with a laser power of 1.5% with the linear fit $\Gamma_s = Dq^2$, D is indicated in the graph. (d) ACFs measured at $q = 0.005 \text{ nm}^{-1}$ for C_{60} (squares) and MEH-PPV:TNF = 1 : 0.15 (circles) in coordinates $\ln I$ vs. t^2 , the lines are linear fits.

$q < 0.023 \text{ nm}^{-1}$ and goes down to 0.55, which is evidence of a transition to sub-diffusion. At high scattering vectors (small spatial scales), the values of β in the blend become close to those of the semidilute pristine polymer (see Fig. 1 (b)). Therefore, one can suggest that the slow dynamics in the blend and the pristine polymer are similar at high q .

For the pristine polymer, the ACF shape and all the fitting parameters (Γ_s , Γ_f , and β) are independent of the laser power, as illustrated in Fig. 1 (b) and (c). Fig. 1(d) and its inset compare the ACFs for MEH-PPV:TNF = 1 : 0.15 and pristine MEH-PPV, measured at different powers of the incident laser beam. In contrast, the ACF in the blends does depend on the laser power. Fig. 2 (c)–(f) illustrate how the slow dynamics parameters, Γ_s , β , and the velocity of ballistic motion decrease with decreasing the laser power. At powers 5% (1 mW) and 1.5% (0.3 mW), fitting by $\Gamma_s(q) \propto Aq^\alpha$ gives $\alpha \sim 4$, which is exactly the same as in the pristine polymer (inset, Fig. 1(c)). At these low powers, the spatial spectra of β in the blends also become similar to that of the pristine polymer; indeed, at any scattering vector, β is smaller than unity and drops to ~ 0.55 with increasing q . We conclude that, at a low laser power, the slow dynamics in the blend becomes similar to those observed in the pristine polymer.

Interestingly, the characteristic time of fast relaxation, τ_f , does not depend on the laser power in the blends, as Fig. 2 (a) and (b) show. At full laser power, the contribution of fast relaxation in the blends is approximately one order of magnitude smaller

($A = 0.1$ in eqn(1)) than that of the slow relaxation, whereas both of the relaxations give similar ($A = 0.4$) contributions to the pristine polymer ACF. Therefore, the slow concentration fluctuations become a dominant relaxation mode in the blends. The relative contribution of fast relaxation in the blends increases with the power decreasing, and, at low power, 5% and 1.5%, the very close contributions of the slow and fast modes in the DLS signal ($A \sim 0.4$ in eqn(1)) are observed, as in the pristine polymer.

B. Fullerene

Fig. 3 presents the DLS data for a C_{60} solution in chlorobenzene. Fig. 3(a) shows the ACFs measured at different laser powers, the solid lines represent fits by the KWW function [eqn (1)]. The insets show the size distributions calculated using the CONTIN software. One can see that the CONTIN distribution includes the only narrow band for 100% (20 mW) laser power. From the KWW fit, we have obtained $A \sim 10^{-4}$ [eqn (1)], which is evidence of the only relaxation process in the fullerene solution. The characteristic relaxation time obtained from the KWW fit corresponds to the only band in the CONTIN distribution.

Fig. 3 (b) and (c) show the spatial spectra of the KWW fit parameters (β and Γ_s) for different laser powers. At small q ($q < 0.023 \text{ nm}^{-1}$) and a laser power of 5% and higher, the dynamics in C_{60} is very similar to that in the polymer blend. Indeed, Γ_s depends linearly on q indicating ballistic motion. At a large

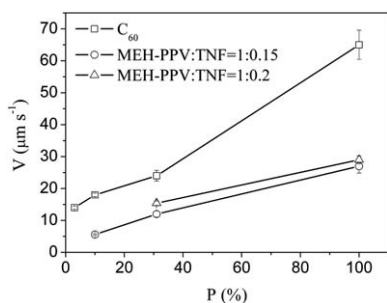


Fig. 4 Convection velocities vs. the laser power for the MEH-PPV:TNF blends and C_{60} . The power 100% corresponds to 20 mW. The lines are guides to the eye.

q ($q > 0.023 \text{ nm}^{-1}$), the dependence $I_s(q)$ diverges down from the linear one. The lower the laser power, the less the divergence is pronounced.

As Fig. 3(b) shows, the Gaussian ACF is also observed in the fullerene sample at a low q . To visually demonstrate the Gaussian shape of the ACFs, Fig. 3(d) plots the ACFs for the C_{60} and MEH-PPV:TNF blend measured at the smallest q in the coordinates $\ln I$ vs. t^2 , with their linear fits. This fits closely follow the experimental data, clearly showing the Gaussian shape of the ACFs.

Upon decreasing the laser power, the ballistic velocity decreases (Fig. 2(c)), this is also observed in the MEH-PPV:TNF blends. Moreover, β decreases with decreasing the laser power and increasing the scattering vector, and this again, is also observed in the MEH-PPV:TNF blends. However, in contrast to the polymer blends, β does not fall below unity in the measured range of the scattering vectors and powers. At the lowest laser power, the dependence $I_s(q)$ can be fitted by a quadratic dependence, $I_s = Dq^2$, (right inset, Fig. 3(c)), and β is about unity and does not depend on q . This indicates the transition from hyperdiffusion to diffusion at decreasing laser power. At the lowest laser power (1.5%), the CONTIN size distribution only includes a wide band with an average hydrodynamic radius of $\sim 430 \text{ nm}$ (inset, Fig. 3(a)). This size could be assigned to the fullerene aggregates in chlorobenzene.^{45–47} The diameter of a fullerene molecule is 0.7 nm ; therefore, we could barely probe the diffusive motion of the individual molecules against the background resulting from the diffusion of the fullerene aggregates. This can explain why the fast diffusive relaxation of individual fullerene molecules is not observed. One can conclude that with decreasing laser power, the inherent thermal molecular dynamics appear in both the fullerene and polymer solutions.

III. Discussion

A. Convection

The slow relaxation in both the polymer blend and fullerene samples appears to be very similar: the hyperdiffusive dynamics accompanied by ballistic motion is observed. The velocity of ballistic motion, V , strongly depends on the laser power; it decreases with decreasing laser power in both the polymer and fullerene samples. Fig. 4 shows the ballistic velocity as a function

of the laser power for the samples with different absorptions: C_{60} and MEH-PPV:TNF blends with different acceptor content. Therefore, it is natural to suggest that the ballistic motion is induced first of all by laser irradiation *via* absorption in the samples at the DLS wavelength (633 nm). The absorptions of all the samples and the corresponding ballistic velocities in chlorobenzene are listed in Table 1. Importantly, the pristine polymer absorption at 633 nm is more than 30 times lower than that of the other samples. This explains why we do not observe ballistic motion in the pristine MEH-PPV. As follows from Table 1, the higher the absorption, the larger the ballistic velocities.

One can suggest that the laser beam absorption in the sample results in its local heating that in turn induces the convective motion. As a result, the laser light is scattered from concentration fluctuations initiated by the convection. We propose that the observed ballistic motion is convective due to a temperature gradient induced by the laser beam. Hence, the measured ballistic velocity is the convective one. By decreasing the laser power, less light is absorbed and a smaller temperature gradient drives the convection. Accordingly, the characteristic convective velocity will be lower and the hyperdiffusion will be less pronounced. Therefore, the laser-induced hyperdiffusion should result in DLS data that is dependent on the laser power. In the gravity field, the convective flow forms a convection roll.³⁵ The DLS signal results from the convection velocity difference within the scattering volume. Moreover, only those components of the convection velocity that are in the plane defined by the incident and scattered beams (*i.e.*, the horizontal plane in our geometry) contribute to the DLS signal.³⁵ This leads to a decrease in the convection contribution at large light scattering vectors (see the next section). The convection driving force, *i.e.*, the laser-induced temperature gradient, is evaluated below (Sec. III C) from the thermal lens experiment.

It is natural to suggest that the Gaussian ACF (*i.e.*, hyperdiffusion with $\beta = 2$) observed at low scattering vectors (*i.e.*, at a large spatial scale) in both the polymer blend and fullerene samples also results from laser-induced convection. This is supported by the fact that the values of β decrease with decreasing laser power. Note that we have observed both the Gaussian ACF and the ballistic motion in the samples with completely different molecular structures: entangled conjugated polymer chains and fullerene aggregates.

As shown earlier, the ACF shape in a laminar flow of scatterers with a linear gradient in their flow velocity can be a Fourier transform of the laser beam intensity profile⁴⁸ and, hence, may not be related to the scatterer fluctuation dynamics. At the same time, the ACF duration should be proportional to the velocity gradient projected on the scattering vector. In our DLS experiment, the laser beam profile is Gaussian, and, therefore, the measured ACF should be Gaussian if we assume that the convection velocity profile within the scattering volume is similar to that of the linear shear field.^{48,49} This assumption is in accordance with the DLS studies on laser-induced motion of absorbing colloidal particles.³⁵ Consequently, we assign the observed Gaussian ACF to the Gaussian laser beam profile, with its duration being determined by the characteristic convection velocity difference over the laser beam aperture. According to the model in Ref. 49 and our DLS data, this velocity difference should be assigned to the measured ballistic velocity. The

convection velocity gradient projected on the scattering vector can be evaluated from the ballistic velocity and the laser beam radius; this gradient is in the range of $0.1\text{--}1\text{ s}^{-1}$.

The earlier DLS studies on absorbing samples^{34–36} showed that the corresponding ACFs include oscillations, which are evidence of convection.³⁵ The relative oscillation amplitude was observed to be about 15%³⁵ and 10%.³⁶ As we have not observed oscillations in our ACFs, we have to analyze the convection in terms of hyperdiffusive dynamics accompanied by ballistic motion. Our convection velocities are in the range of $5\text{--}60\text{ }\mu\text{m s}^{-1}$ for an absorbed laser power of $1\text{--}12\text{ mW}$, correspondingly. They are one order of magnitude less than obtained earlier,^{35,36} and this is in accordance with the one order of magnitude lower power used (20 mW) at similar absorbancies. One could expect that the hyperdiffusive dynamics observed in solutions absorbing at the DLS wavelength can be used as a probe for weak laser-induced convection.

B. Hyperdiffusive dynamics in polymer blend and fullerene solutions

We have observed the very similar hyperdiffusive dynamics in the diverse samples, the conjugated polymer blend and the fullerene solutions. The above analysis suggests that the sample absorption mainly controls the observed hyperdiffusive dynamics. Nevertheless, one can expect that the different molecular structures of the polymer blend and the fullerene could be exhibited in the hyperdiffusive dynamics. In this section, we compare the hyperdiffusive dynamics in the polymer and fullerene samples.

We have observed that the hyperdiffusive dynamics is more pronounced in the fullerene sample compared with the polymer blends. Firstly, the q -dependence of the exponent β falls to unity in polymer blends more quickly than in the fullerene sample (Fig. 2(e,f) and 3(b)). Secondly, the characteristic convective velocity in the fullerene sample is considerably larger than in the polymer blends for a wide range of laser powers (Fig. 4). Thirdly, the convection becomes negligible in the fullerene sample at a lower laser power (1.5%) compared to the polymer blends (5%). We relate these differences first of all to the difference in the sample absorbance (Table 1). However, although the fullerene sample absorbance is 1.6 times higher than that of the MEH-PPV:TNF = 1 : 0.15 blend, the ballistic velocity is ~ 2.4 times higher. Therefore, apart from the absorbance, there should be at least one other aspect that influences the hyperdiffusive dynamics. This reason could be related to the different inherent molecular dynamics in the fullerene and the semidilute conjugated polymer blend. Indeed, the fullerene aggregates can freely diffuse in solution,^{45–47} whereas the conjugated polymer chains are entangled, with their fluctuations interconnected. It is natural to expect that the isolated fullerene aggregates are more easily involved in convection than the entangled polymer chains. Because of this, the hyperdiffusive dynamics can be more pronounced in the fullerene sample.

At large scattering vectors, differences in the hyperdiffusive dynamics of the polymer blend and fullerene sample are also observed: the $I_s(q)$ dependence measured at high laser powers (100% and 28%) deviates from the straight line and tends towards shorter relaxation times in the polymer blend (Fig. 2(c)) and longer ones in the fullerene sample (Fig. 3(c)). The convection

contribution to the ACF is proportional to the scalar product of vectors q and V .³⁵ As the convective velocity is perpendicular to the wave vector of incident laser beam,³⁵ the higher the scattering vector, the lower the convective contribution to the DLS signal: the vectors q and V are almost collinear at small scattering angles ($\theta \sim 20^\circ\text{--}30^\circ$) and almost perpendicular at high ones ($\theta \sim 140^\circ\text{--}150^\circ$). Therefore, at high scattering vectors ($\theta > 90^\circ$), the inherent thermal molecular motions become more apparent when competing with convection. This could explain the observed deviation of $I_s(q)$ from the linear dependence at high q . In the polymer blend and fullerene sample, these deviations are opposite and could be assigned for their different inherent dynamics. One could suppose that the slow dynamics of the entangled polymer chains, characterized by their q^4 -dependence in the pristine polymer (Fig. 1(c)), becomes apparent at high q in the blend (Fig. 2(c) and (d)). The q^4 -dependencies are also observed in the blends at low powers as well as in the pristine polymer (see Sec. III D). The deviation in the fullerene sample (inset, Fig. 3(a)) is harder to assign as we have no sufficient information about the structure of the scatterers which could be fullerene/carbon aggregates or other unidentified species. More careful understanding of the spatial spectrum, $I_s(q)$, at the high scattering vectors in the fullerene sample requires additional studies.

Upon decreasing the laser power and/or increasing the scattering vector, β decreases from two to unity and 0.55 for the fullerene and polymer samples, respectively. This β -range could be assigned to the transition from the deterministic convection to random inherent fluctuations (on ref. 35, *i.e.*, diffusion for C_{60} and subdiffusion for the polymer blends).

C. Laser-induced temperature gradient

As suggested above, the convection resulting from the local heating of the liquid sample is a main reason for the hyperdiffusive dynamics observed in our DLS studies. In this section, we further substantiate our conclusion by a thermal lens experiment, the observation of the laser beam transmitted by an absorbing sample in the far field. From this experiment the local temperature difference driving the convection is estimated from the analysis of the laser beam divergence.

We have observed that concentric rings appear in the far field of the laser beam, transmitted by the absorbing polymer and

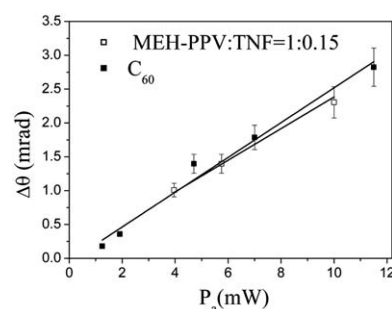


Fig. 5 Laser beam divergence $\theta - \theta_0$ vs. the absorbed power P_a for the MEH-PPV:TNF = 1 : 0.15 (open squares) and fullerene (full squares) samples. The lines are fitting curves according to eqn (2) with the parameters $(\partial n/\partial T)(1/\pi a \kappa) = 0.23 \pm 0.01\text{ rad W}$ for the polymer blend and $(\partial n/\partial T)(1/\pi a \kappa) = 0.26 \pm 0.03\text{ rad W}$ for the fullerene.

fullerene samples. This phenomenon is well known as the thermal lens effect. It develops in the absorbing media, appearing as a result of self-phase modulation.^{35,50} The temperature gradient drives the convective motion of scatterers from the heated regions to cooler ones.^{35,36}

The divergence angle θ of the laser beam after passing through the samples, has been measured as a function of the absorbed power P_a . It is displayed as:⁵¹

$$\theta = \theta_0 + \frac{\partial n}{\partial T} \frac{P_a}{\pi a \kappa}, \quad (2)$$

where θ_0 is the initial beam divergence that was about 0.6 mrad, a is the radius of the beam at the entrance of the cell, and κ is the thermal conductivity. The local radial change in refractive index Δn can be calculated as:⁵²

$$\Delta n = \frac{\partial n}{\partial T} \Delta T = \frac{\partial n}{\partial T} \frac{P_a}{4\pi l \kappa}, \quad (3)$$

where l is the cell optical length. Fig. 5 presents the laser-induced changes in divergence, $\Delta\theta = \theta - \theta_0(P_a)$, for MEH-PPV:TNF = 1 : 0.15 and fullerene samples with the fits according to eqn (2). The refractive index of chlorobenzene ($n = 1.52$) was also taken into account. The corresponding values of Δn and $(\partial n/\partial T)/\kappa$ were estimated for $a = 0.8$ mm, $l = 5$ mm, and are listed in Table 1. The values of Δn and $(\partial n/\partial T)/\kappa$ are close to those obtained earlier for a fullerene solution in toluene.⁵² The values of Δn are smaller in the polymer blend than in the fullerene solution in accordance with the lower absorption of the MEH-PPV:TNF = 1 : 0.15 blend. The lower the absorption, the lower the temperature gradient and the local changes in Δn . The local temperature change can be estimated from the fits in Fig. 5 as:

$$\Delta T = \frac{\Delta n}{(\partial n/\partial T)(1/\kappa)} \cdot \frac{1}{\kappa}, \quad (4)$$

As the concentrations of the solutions are low (1 g L⁻¹ for C₆₀ and 4 g L⁻¹ for MEH-PPV:TNF blend), one can assume that the thermal conductivities of the fullerene and MEH-PPV:TNF solutions are close to that of solvent, *i.e.*, chlorobenzene. Therefore, we suppose that the thermal conduction is realized mainly by solvent molecules. By using the thermal conductivity of chlorobenzene $\kappa = 0.128$ W m⁻¹ K⁻¹ (for 20°), the calculated values of ΔT according to eqn (4) are listed in Table 1, we conclude that the laser-induced heating of about 0.1–0.2 K results in convection with velocities of 5–60 μm s⁻¹. The authors directly measured the temperature difference in the absorbing solution of colloidal particles containing tiny gold clusters and showed that the convection velocity ~ 1 mm s⁻¹ was induced by a temperature difference of ~ 6 K.³⁵ Accordingly, the ratio $V/\Delta T$ is in good agreement with the earlier data.

At low laser powers, we have not observed any laser-induced beam expansion and concentric rings in the far field. This is in accordance with the DLS data, the disappearance of convection also occurs at these low powers.

In summary, we have found that the convection induced by absorption in the samples appears itself in the DLS measurements as hyperdiffusion with the exponent, β , reaching 2. The convective velocities have been determined as velocities of ballistic motion for fullerene and conjugated polymer blend samples and are about 60 and 20 μm s⁻¹ at an absorbed, laser

power of ~ 12 and 10 mW, respectively. The temperature differences driving these velocities have been evaluated to be about 0.2 and 0.1 K, correspondingly.

D. Molecular dynamics at low laser powers

In this section, we discuss the DLS data measured at low laser powers P . Upon decreasing P down to 5% (for MEH-PPV:TNF) and 1.5% (for C₆₀), the convection disappears and the inherent thermal molecular dynamics becomes apparent. In fact, the DLS data in the polymer blend at decreasing laser powers becomes very similar to those in the pristine polymer in which the absorbance at the DLS excitation wavelength is low (see Table 1 and Fig. 1(c)); β becomes P -independent, the β spatial spectra (Fig. 2(e)) become similar to that of the pristine polymer, β decreases and passes through unity indicating the transition from hyper- to subdiffusion (Fig. 1(b)), and the spatial spectrum in the blend is well approximated as $I_s(q) \propto q^4$ (inset, Fig. 2(c)). These similarities indicate that in the blend the light is scattered from the fluctuations of entangled π -conjugated chains without any noticeable contribution from convection. Furthermore, the contribution of fast relaxation (blob fluctuations) increases with decreasing laser power. At $P = 5\%$ and 1.5% the ratios of fast and slow contributions are the same as in the pristine polymer ($A \sim 0.4$ in eqn(1)). One can suggest that at $P \leq 5\%$ in the blend, the local heating is low, so convection can be neglected and hence the inherent polymer chain dynamics can be probed.

Interestingly, the diffusivities corresponding to the fast relaxation are independent of the laser power in the blends and are close to that of the pristine polymer. One can conclude that the fast dynamics assigned to the diffusive fluctuations in blobs have not been changed upon acceptor addition.

In the fullerene sample, decreasing the laser power results in decreasing the exponent β from two to unity. At the lowest laser power (1.5%), β is independent of the scattering vector and equal to unity (Fig. 3(b)), indicating common diffusive fluctuations. Moreover, the spatial spectrum demonstrates the quadratic dependence ($I_s = Dq^2$) with diffusivity $D = (0.80 \pm 0.04) \times 10^{-8}$ cm² s⁻¹ (right inset, Fig. 3 (c)). This corresponds to diffusing particles with a hydrodynamic radius of 240 ± 14 nm, according to the Stokes–Einstein relation. The CONTIN software gives the only wide band with an average hydrodynamic radius of ~ 430 nm (inset, Fig. 3(a)) with the full width at half maximum of about 1000 nm. This indicates a strong polydispersity for the fullerene sample. One could suppose that fullerene aggregates and maybe other carbon species with hydrodynamic radii in the range 200–1200 nm are present in the fullerene sample at low concentrations. It is well known that fullerenes aggregate in most organic solvents.^{45–47} As the fullerene solution was filtered by PTFE (Millex 0.45 μm), one should expect the absence of large particles (>450 nm) in it. However, one could suppose that the large aggregates are also formed after filtration. These large particles could be visible in the data as the DLS method is very sensitive to large species because the scattering intensity scales to the third degree of the particle size.⁵³ This could explain why we do not observe the diffusive fluctuations of individual fullerene molecules on the background, resulting from the light scattered from the large particles. Note that in this study, it was not important to avoid

fullerene aggregation. We used chlorobenzene C_{60} solutions as just another sample (in addition to the polymer ones) absorbing at the DLS wavelength to establish the origin of the observed hyperdiffusion.

Thus, at low laser power, the convection is negligible, and the inherent thermal molecular motion could be probed. In the polymer blend, fluctuations of polymer chains are dominant, showing sub-diffusive dynamics similar to those in the pristine polymer. In the fullerene sample, the dynamics is diffusive, indicating the presence of large particles. The laser power at which the convection disappears and the inherent thermal motions could be probed depends on the sample absorbance and its type. One can determine this power by measuring the dependence of hyperdiffusion dynamics on it.

IV. Experimental

MEH-PPV (Sigma-Aldrich, $M_n = 86\,000$, $M_w = 420\,000$) and TNF were dissolved separately in chlorobenzene at initial concentrations of 4 g L^{-1} . The overlap concentration in MEH-PPV solution was found to be about 1.5 g L^{-1} as described in the DLS data, hence, the polymer solution under study is semidilute. The TNF solution was filtered by PTFE (Millex $0.45\text{ }\mu\text{m}$), and then the MEH-PPV and TNF solutions were mixed at the MEH-PPV:TNF molar ratio of $1 : 0.15$ and $1 : 0.2$ per polymer unit. Fullerene (99.98%) was dissolved in chlorobenzene at a concentration of 1 g L^{-1} and filtered by PTFE (Millex $0.45\text{ }\mu\text{m}$). The optical absorption coefficients of the samples were measured by using a fiber-coupled spectrophotometer (Avantes) and are given in Table 1.

The DLS studies were done with the use of a correlator-goniometer system ALV-CGS-5000/6010 (Langen, Germany) equipped by a He-Ne laser radiating at a wavelength of 633 nm , the power at the sample was 20 mW . We refer to this power as the 100% one. A cylindrical glass cuvette with the sample was placed in a toluene bath to avoid reflections from the cuvette walls. The bath was kept at a constant temperature of $20\text{ }^\circ\text{C}$. The cuvette length was 0.8 cm . The intensity ACF was measured at different scattering angles from 20° to 150° corresponding to the scattering vectors $q = 0.005\text{--}0.03\text{ nm}^{-1}$. The ACFs were approximated by the KWW function [eqn(1)]. The inaccuracy of the KWW fitting parameters was less than 5% for all the samples. The angular dependencies for different relaxation decays I were approximated by power function $I \sim q^\alpha$ to determine the fitting parameter α and the corresponding relaxation type. We also used the CONTIN procedure to analyze the type of relaxations; however, the inaccuracy of the CONTIN for 100% laser power reached 40%. Because of this, for 100% laser power, we used the CONTIN time relaxation distribution only for the qualitative analysis. The CONTIN distributions in scatterer sizes could be obtained from the relaxation times by scaling with the use of the Stokes–Einstein relation.¹⁶ The latter gives either the correlation length, or hydrodynamic radius, depending on the corresponding molecular relaxation.

The profile of the transmitted laser beam was studied in the far field with the power on the sample of 16 mW . The cell length was 1 cm for the MEH-PPV:TNF blends and 0.5 cm for the C_{60} solution.

V. Conclusion

We have established the origin of hyperdiffusive dynamics in absorbing polymer and fullerene samples probed by DLS. The hyperdiffusive dynamics can appear as a result of laser-induced convection caused by the local heating of the samples absorbing at the DLS wavelength. The similar hyperdiffusive dynamics was observed in diverse samples, namely in conjugated polymer–acceptor and fullerene solutions, and is accompanied by the ballistic motion of light scatterers. The relation between the laser-induced convection and hyperdiffusion have been studied, and we conclude that the measured ballistic velocities are related to the convective ones. As a result, on the one hand, the hyperdiffusion could be used to probe weak laser-induced convection. On the other hand, the laser-induced convection can mask the inherent thermal molecular fluctuations in the absorbing samples. However, we have shown that the convection can be avoided both in the polymer and fullerene samples by decreasing the absorbed laser power. Therefore, with the proper caution, the DLS technique could give information about the inherent thermal molecular dynamics in samples absorbing at the DLS wavelength.

VI. Acknowledgement

We thank M.S. Pshenichnikov, V.V. Bruevich and S.A. Zapunidi for fruitful discussions. This work was supported by the Ministry of Education and Science of Russian Federation (contracts # 02.740.11.5155, 02.523.11.3020, 16.740.11.0064 and 16.740.11.0249) and the Russian Foundation for Basic Research (project # 11-02-01074a).

VII. Bibliographic references

- 1 W. Brown, *Dynamic Light Scattering, the Methods and Applications*. Clarendon Press, Oxford, 1993.
- 2 F. Brochard and P. G. de Gennes, *Macromolecules*, 1977, **10**, 1157.
- 3 W. Brown and T. Nicolai, *Colloid Polym. Sci.*, 1990, **268**, 997–990.
- 4 W. Brown and K. Mortensen, *Macromolecules*, 1998, **21**, 420.
- 5 P. Stepanek and W. Brown, *Macromolecules*, 1998, **31**, 1889–1897.
- 6 J. Li, W. Li, H. Huo, S. Luo and C. Wu, *Macromolecules*, 2008, **41**, 901.
- 7 M. Shibayama and M. Okamoto, *J. Chem. Phys.*, 2001, **115**(9), 4285–4291.
- 8 T. Matsunaga and M. Shibayama, *Phys. Rev. E: Stat., Nonlinear, Soft Matter Phys.*, 2007, **76**(3), 030401.
- 9 M. Shibayama, T. Karino, Y. Domon and K. Ito, *J. Appl. Crystallogr.*, 2007, **40**, S43–S47.
- 10 N. Osaka, S. Takata, T. Suzuki, H. Endo and M. Shibayama, *Polymer*, 2008, **49**, 6.
- 11 C. Esquenet, P. Terech, F. Boue and E. Buhler, *Langmuir*, 2004, **20**, 3583.
- 12 M. Shibayama, S. Ozeki and T. Norisuye, *Polymer*, 2005, **46**, 2381–2388.
- 13 T. Norisuye, T. Morinaga, Q. Tran-Cong-Miyata, A. Goto, T. Fukuda and M. Shibayama, *Polymer*, 2005, **46**, 1982–1994.
- 14 A. N. Semenov, *Phys. A*, 1990, **166**, 263.
- 15 A. N. Semenov, *Sov. Phys. JETP*, 1986, **63**(4), 717.
- 16 L. Cipelletti, S. Manley, R. C. Ball and D. A. Weitz, *Phys. Rev. Lett.*, 2000, **84**, 2275.
- 17 A. Yu. Grosberg and A. R. Khokhlov, *Statistical Physics of Macromolecules*. AIP Press, NY 1994.
- 18 M. Adam and M. Delsanti, *Macromolecules*, 1985, **18**, 1760.
- 19 B. Ewen, D. Richter, B. Farago and B. Stühn, *J. Non-Cryst. Solids*, 1994, **1023**, 172–174.

- 20 L. Cipelletti, L. Ramos, S. Manley, E. Pitard, D. A. Weitz, E. E. Pashkovski and M. Johansson, *Faraday Discuss.*, 2003, **123**, 237–251.
- 21 H. Y. Guo, G. Bourret, M. K. Corbierre, S. Rucareanu, R. B. Lennox, K. Laaziri, L. Piche, M. Sutton, J. L. Harden and R. L. Leheny, *Phys. Rev. Lett.*, 2009, **102**(7).
- 22 M. L. Ruegg, A. J. Patel, S. Narayanan, A. R. Sandy, S. G. J. Mochrie, H. Watanabe and N. P. Balsara, *Macromolecules*, 2006, **39**(25), 8822–8831.
- 23 P. Falus, S. Narayanan, A. R. Sandy and S. G. J. Mochrie, *Phys. Rev. Lett.*, 2006, **97**(6).
- 24 R. A. Narayanan, P. Thiyagarajan, S. Lewis, A. Bansal, L. S. Schadler and L. B. Lurio, *Phys. Rev. Lett.*, 2006, **97**(7).
- 25 S. Narayanan, D. R. Lee, A. Hagman, X. F. Li and J. Wang, *Phys. Rev. Lett.*, 2007, **98**(18).
- 26 C. Caronna, Y. Chushkin, A. Madsen and A. Cupane, *Phys. Rev. Lett.*, 2008, **100**(5), 055702–055704.
- 27 M. Bellour, A. Knaebel, J. L. Harden, F. Lequeux and J. P. Munch, *Phys. Rev. E: Stat. Phys., Plasmas, Fluids, Relat. Interdiscip. Top.*, 2003, **67**(3).
- 28 A. Fluerasu, A. Moussaid, A. Madsen and A. Schofield, *Phys. Rev. E: Stat., Nonlinear, Soft Matter Phys.*, 2007, **76**(1), 010401–010404.
- 29 A. Madsen, R. L. Leheny, H. Guo, M. Sprung and O. Czakkel, *New J. Phys.*, 2010, **12**, 055001.
- 30 K. Laszlo, A. Fluerasu, A. Moussaid and E. Geissler, *Soft Matter*, 2010, **6**, 4335–4338.
- 31 A. Duri and L. Cipelletti, *Europhys. Lett.*, 2006, **76**(5), 972–978.
- 32 J.-P. Bouchaud and A. Georges, *Phys. Rep.*, 1990, **195**, 127.
- 33 J. P. Bouchaud and E. Pitard, *Eur. Phys. J. E: Soft Matter Biol. Phys.*, 2001, **6**(3), 231–236.
- 34 H. Oikawa, H. Nakanishi and K. Takeda, *J. Macromol. Sci., Part B: Phys.*, 2000, **39**(1), 15–26.
- 35 W. Schäertl and C. Roos, *Phys. Rev. E: Stat. Phys., Plasmas, Fluids, Relat. Interdiscip. Top.*, 1999, **60**(2), 2020–2028.
- 36 A. Sehgal and T. A. P. Seery, *Macromolecules*, 1999, **32**, 7807–7814.
- 37 A. A. Bakulin, S. G. Elizarov, A. N. Khodarev, D. S. Martyanov, I. V. Golovnin, D. Y. Parashuk, M. M. Triebel, I. V. Tolstov, E. L. Frankevich, S. A. Arnautov and E. M. Nechvolodova, *Synth. Met.*, 2004, **147**(1–3), 221–225.
- 38 A. A. Bakulin, A. N. Khodarev, D. S. Martyanov, S. G. Elizarov, I. V. Golovnin, D. Y. Parashuk, S. A. Arnautov and E. M. Nechvolodova, *Doklady Chemistry*, 2004, **398**(Part 2), 204–206.
- 39 D. Y. Parashuk, S. G. Elizarov, A. N. Khodarev, A. N. Shchegolikhin, S. A. Arnautov and E. M. Nechvolodova, *JETP Lett.*, 2005, **81**(9), 467–470.
- 40 M. Okamoto, T. Norisuye and M. Shibayama, *Macromolecules*, 2001, **34**(24), 8496–8502.
- 41 P. G. De Gennes, *Scaling Concepts in Polymer Physics*. Cornell University Press: Ithaca, NY, 1979.
- 42 E. J. Amis and C. C. Han, *Polymer*, 1982, **23**, 1403.
- 43 Y. Einaga, A. Itaya and M. Takaoka, *Polymer*, 2002, **43**, 4869–4877.
- 44 T. Tanaka, L. O. Hocker and G. B. Benedek, *J. Chem. Phys.*, 1973, **59**, 5151.
- 45 T. P. Martin, U. Näher, H. Schaber and Z.U., *Phys. Rev. Lett.*, 1993, **70**, 3079–3082.
- 46 W. J. Blau, H. J. Byrne, D. J. Cardin, T. J. Dennis, J. P. Hare, H. W. Kroto, R. Taylor and D. R. M. Walton, *Phys. Rev. Lett.*, 1991, **67**, 1423–1425.
- 47 R. V. Honeychuck, T. W. Cruger and J. Milliken, *J. Am. Chem. Soc.*, 1993, **115**, 3034.
- 48 R. T. Foister and T. G. M. Van de Ven, *J. Fluid Mech.*, 1980, **96**(1), 106–132.
- 49 G. G. Fuller, J. M. Rallison, R. L. Schmidt and L. G. Leal, *J. Fluid Mech.*, 1980, **100**(3), 555–576.
- 50 Y. R. Shen, *Principles of Nonlinear Optics*. Wiley-Interscience; 1st edn, 1984.
- 51 S. A. Akhmanov, D. P. Krindach, A. V. Migulin, A. P. Sukhorukov and R. V. Khokhlov, *IEEE J. Quantum Electron.*, 1968, **4**, 568.
- 52 M. Ahmed and T. Riffat, *Journal Of Modern Optics*, 2004, **51**(11), 1663–1670.
- 53 E. Tarassova, V. Aseyev, A. Filippov and H. Tenhu, *Polymer*, 2007, **48**(15), 4503–4510.